

# Plasmonic nanostructures in aperture-less scanning near-field optical microscopy (aSNOM)

Ralf Vogelgesang<sup>\*1</sup>, Jens Dorfmueller<sup>1</sup>, Ruben Esteban<sup>2</sup>, R. Thomas Weitz<sup>1</sup>, Alexandre Dmitriev<sup>3</sup>,  
and Klaus Kern<sup>1,4</sup>

<sup>1</sup> Max Planck Institut für Festkörperforschung, Heisenbergstr. 1, 70569 Stuttgart, Germany

<sup>2</sup> Laboratoire EM2C, Ecole Centrale Paris, CNRS, Grande voie des Vignes, 92295 Chatenay-Malabry Cedex, France

<sup>3</sup> Bionanophotonics at Applied Physics, Chalmers University of Technology, 41296 Göteborg, Sweden

<sup>4</sup> Institut de Physique des Nanostructures, Ecole Polytechnique Fédérale de Lausanne, 1015 Lausanne, Switzerland

Received 30 April 2008, revised 18 June 2008, accepted 19 June 2008

Published online 29 August 2008

PACS 68.37.Uv, 71.36.+c, 71.45.Gm, 78.67.-n

\* Corresponding author: e-mail r.vogelgesang@fkf.mpg.de

Apertureless scanning near-field optical microscopy offers superb spatial resolution, but interpreting the recorded signal can still be a challenge. Especially images of eigenmodes in plasmonic nanostructures are very often obscured by concurrent scattering from the tip and/or coupling effects in the tip-sample system. We show here how the use of orthogonal polarizations in excitation and detection affords us with an ele-

gant method to map near-fields of plasmonic eigenmodes and other optical phenomena. We demonstrate with a variety of samples possible applications of this cross-polarization scheme, such as verification of functional nanooptical structures, systematic studies of localized and propagating plasmonic eigenmodes, and their susceptibility to disturbance from structural defects.

© 2008 WILEY-VCH Verlag GmbH & Co. KGaA, Weinheim

**1 Introduction** It has long been appreciated that the metal-dielectric interface gives rise to collective charge density-electromagnetic field oscillations known as the surface plasmon polaritons [1]. In the case of extended interfaces, these can be characterized as propagating wave-like phenomena whose associated wavevectors exhibit well-known continuous dispersion relations. Typically, in the direction normal to the surface, the field strength drops off exponentially and the plasmonic excitations are thus localized in one direction. With the advent of modern nanofabrication techniques it has become possible to manufacture metallic structures with typical dimensions in the few nm to  $\mu\text{m}$  regime. Such nanostructures introduce not only additional confinement in the other two spatial dimensions. In addition, they typically exhibit new resonances in the frequency domain.

This combination is attractive in many ways, as the design of such structures can be very well controlled and thus both the spatial as well as the spectroscopic characteristics may be fine-tuned to achieve desired goals. For example, highly efficient nano-scopic antenna structures that operate

at optical frequencies can be utilized as transducers of local optical phenomena into detectable far-field signals [2] or, conversely, to excite localized optical processes with high spatial selectivity [3-7]. Single molecule spectroscopy, light-induced chemical reactions, opto-electronic, thermal, and many other processes can be applied in a large variety of ways. In these fields, we find a growing number of applications of isolated plasmonic structures playing integral roles as parts of devices. Another exciting application of plasmonic structures are collective phenomena of arrays of individual structures – be they periodic in space or only with short-ranged order. Perhaps most prominently in recent years, the possibility of so-called negative index or left-handed optical materials has been studied extensively [8-12]. With a lack of evident atomic or molecular building blocks suggesting themselves, arrays of nanostructures that exhibit strongly resonant eigenmodes due to sub-wavelength structures are excellent candidates.

To study and characterize the optical properties of these and related structures, local microscopy of optical properties is much needed to complement far-field-

spectroscopic information, which mostly characterizes the frequency-dependence of resonances. Conventional confocal microscopy does not answer all questions in this context, due to its inherently limited spatial resolution. A number of microscopy techniques utilize electronic interactions: for example, cathodoluminescence and electron-energy loss spectroscopy offers the excellent spatial resolution of scanning electron microscopes [13, 14]. However, the need for vacuum conditions and usually conductive samples and/or substrates are serious limitations. Also, these techniques typically characterize the magnitude of local optical field vectors, but not direction or phase.

This kind of information is chiefly accessible by purely optical means, i.e. one of the variety of (scanning) near-field optical microscopy techniques [15-20]. In this context a notable demonstration of feasibility has been given in 2003 [21], where a carbon nanotube was used as local probe to image optical dipole fields of small resonant gold disks. This kind of unusual probe is small enough not to disturb the plasmonic resonances, so that eigenmode mapping becomes possible, albeit at the expense of drastically reduced scattering efficiency due to the minute volume.

In that work, the authors used a parallel polarization scheme: both incident and scattered radiation are p-polarized, which leads to the simultaneous excitation of sample and probing tip. Under these conditions, a probing tip that is a stronger scatterer itself, such as off-the-shelf silicon AFM probes, hinders the straightforward interpretation of the total scattering signal. The interference of simultaneously scattered radiation from sample and tip is difficult to disentangle. If a significant mutual excitation of sample and tip has to be suspected, the interpretation is yet more difficult. In the worst case, which might be given for metallic tips, probe and sample form a strongly coupled system with new eigenmodes. The resulting microscopic images most likely require supporting numerical calculations for interpretation.

We have introduced a simple, yet crucial modification to the approach, utilizing the polarization responses of

probing tip and sample. The combination of s-polarized excitation radiation with p-polarized analysis of the scattered radiation largely de-couples the tip and sample. This allows one to interpret the scattering signal as the product of a linear chain of causes and actions: the s-polarized incident radiation excites mainly the sample. The tip is polarisable mainly along the surface normal [22-24]. Whenever the localized plasmonic eigenmode exhibits strong vertical components, these excite the probing tip, which then scatters p-polarized light off towards the detector. Thus, the recorded signal is seen as directly related to the local field components parallel to the probing tips shaft. As another advantage, much of the parasitic background signal is suppressed. Using an interferometric detection scheme, we can access both amplitude and phase [25-27].

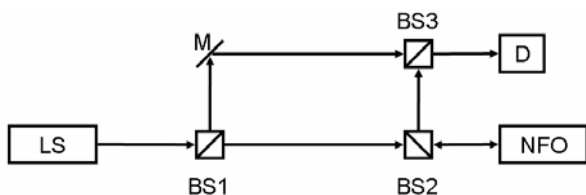


**Figure 1** The experimental scheme. LS: source for coherent monochromatic laser radiation. Beam splitters BS1-3 form a Mach-Zehnder type interferometer with minimal back coupling of radiation into the resonator cavity of the laser. The polarization state in each interferometer arm can be separately controlled. M: mirror. NFO: near-field optical interaction region containing excitation and collection foci, oscillating probe tip and sample. D: detector. The electric signal is de-modulated with a lock-in detector.

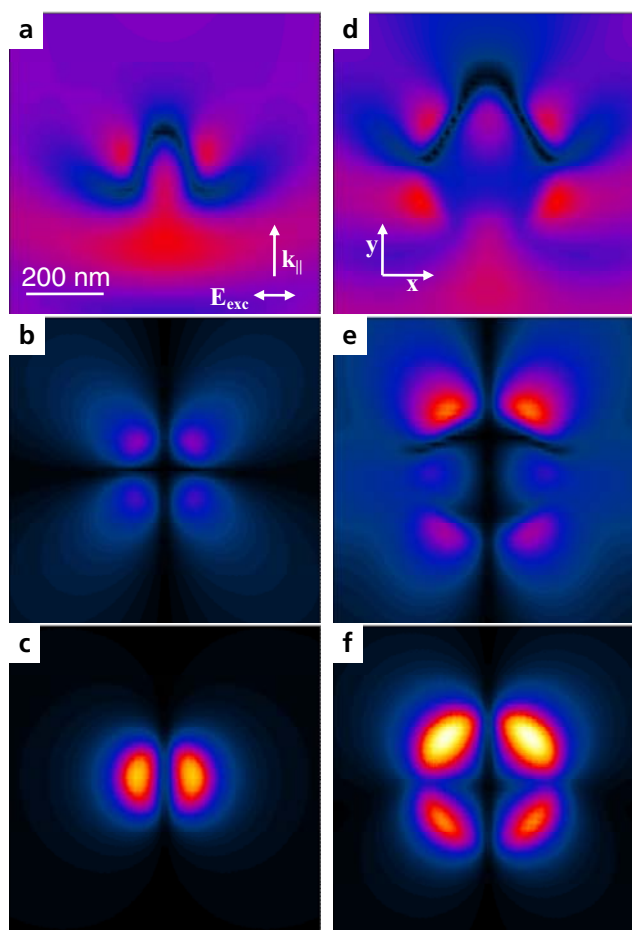


**Figure 2** Illustration of field distributions associated with dipolar and quadrupolar plasmonic eigenmodes of disk-shaped metal structures. 800 nm, s-polarized plane wave excitation is assumed at an incidence angle of 70 degree with respect to the surface normal. The wavevector component parallel to the sample surface is indicated in (a). Shown are the field strengths in the plane 30 nm above a gold disk of 175 nm diameter (b-d) and 350 nm diameter (e-g):  $E_x$  in (b,e),  $E_y$  in (c,f),  $E_z$  in (d,g). All images are shown in the same linear lateral and colour scale.

In the following, we give several examples of applications of our cross-polarized apertureless scanning near-field optical microscopy to the study of localized plasmonic eigenmodes. We show by comparison with numerical simulations and simple theoretical considerations that excellent agreement with theory can be achieved. The lateral resolution is limited by the geometry of the tip apex to about 10 nm.

**2 Materials and methods** Nanostructures preparation has been done using varied methods. Most frequently, nanostructures are fabricated by state-of-the-art electron beam lithography. This top-down method is readily capable of producing structures with defined geometries of a few tens of nm. For the present work, heavily doped silicon wafers coated with 100 nm thermal SiO<sub>2</sub> are utilized as substrates. For the electron beam lithography we use a standard double layer poly(methyl methacrylate) resist with a thickness of 200 nm, an electron energy of 20 keV, and an electron beam dose of 270  $\mu\text{C}/\text{cm}^2$ . Development in a mixture of methyl-isobutyl-ketone:isopropanol (1:3) and thermal metal evaporation of 0.5 nm Ti/20 nm Au, subsequent lift-off in n-methyl-2-pyrrolidone finishes the structures.

An alternative, bottom-up approach to nanofabrication, called hole-mask colloidal lithography (HCL) was also employed [28, 29]. Here, a suspension of charged colloids (polystyrene beads) of specified diameters is drop-cast onto the surface of an oppositely charged thin polymer film. The geometrical shadows of the beads define holes in a subsequently applied thin metallic film, which may then be used as a mask for evaporation of desired metals. After removal of the polymer films carrying the thin metallic mask free-standing, surface supported nanostructures are formed, whose locations on the surface are short range ordered, but over macroscopic distances appear completely random. A third sample preparation technique is focussed ion beam (FIB) milling, which allows to create structures that are “inverse” to those of the previous two methods, e.g., round holes instead of disks or slots instead of wires. All microscopy images were recorded with a home-built apertureless scanning near-field optical microscope [30] (Fig. 1). Excitation of samples is done with monochromatic radiation derived from tunable laser sources (either a Verdi-18 pumped 899 Ti:Sapphire unit from Coherent or an OS4000 optical parametric oscillator from Linos). The incident light is incident at an angle of 70 degrees off the sample surface normal, focussed with an NA = 0.25 aspheric lens, and the backscattered light collected by the same lens. The near-field optical interaction between the sample and a commercial atomic force microscope (M5 by Park Scientific) is modulated by the tip oscillation in non-contact mode (vertically above the sample with a typical amplitude of 5–40 nm). Homodyned, two-step phase shifting interferometry is used to amplify the signal and to retrieve optical amplitude as well as phase information. We use a Mach-Zehnder type interferometer to conveniently manipulate the polarization states of excitation, signal, and

reference arms independently. The recorded signal is demodulated at the second or third harmonic of the fundamental tip oscillation frequency. Commercial bare silicon tips are used as probes, often etched to remove the native oxide layer, but also with the oxide near-field optical imaging is possible.

For simulation, we use the Max-1 package [31] to obtain the elastic scattering response of given structures to monochromatic excitation. It is based on the multiple-multipole technique [32], dividing space into piecewise homogeneous domains of specific material properties, expanding the fields in each domain into known solutions for the three-dimensional bulk Maxwell equations (such as multipole fields), and minimizing the matching errors in the boundary conditions at domain interfaces to find the best expansion parameters.

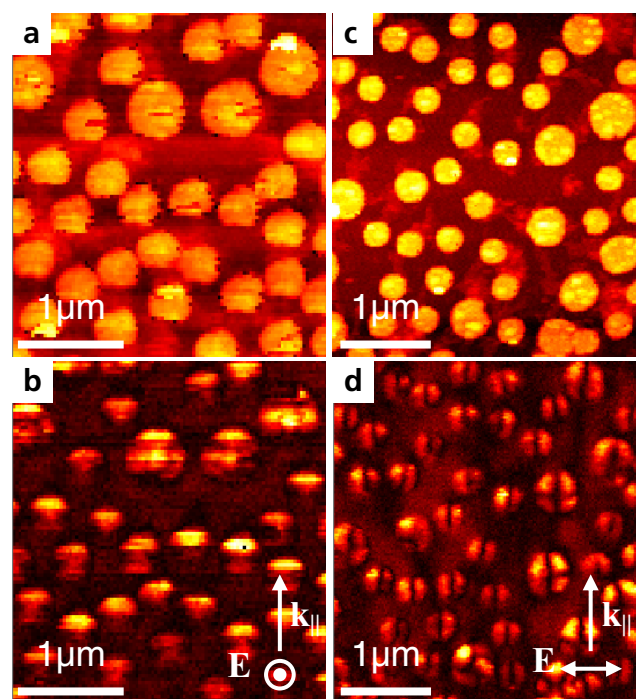


**Figure 3** Topographic (a,c) and near-field (b,d) optical images of a sample containing short-range ordered arrays of two HCL Au disk species of 140 and 300 nm diameter. The polarization of the exciting electric field is indicated in (b,d) together with the wavevector component parallel to the sample surface.

**3 Results and discussion** To illustrate the main features and possibilities of our approach to plasmonic eigenmode imaging we discuss first some results obtained with gold nanodisks. Thanks to their elementary geometry, the expected plasmonic eigenmodes are very intuitive, as illustrated by numerical simulations in Figure 2. We assume a glass substrate support and air forming an effective dielectric host medium of homogeneous index of refraction 1.25. For a particular excitation frequency (here corresponding to 800 nm vacuum wavelength) metallic nano particles embedded in a dielectric medium respond strong-

est with the plasmonic eigenmode whose (complex-valued) eigenfrequency is closest. An s-polarized planar wave excites a dipolar response in the smaller diameter (175 nm) disk, while it gives rise to a quadrupolar response in the larger disks (350 nm). The corresponding field components  $E_x$ ,  $E_y$ , and  $E_z$  are presented in Figs. 2a-c and Figs. 2d-f, respectively. Shown are the values obtained in an xy plane 30 nm above the metallic nanostructures, which is chosen to represent the near-field optical probe in our experiments.

We note the importance of retardation effects. On the one hand, it is the propagation of the exciting wave in the y-direction that breaks the symmetry between “front” and “back”, thus enabling the excitation of quadrupolar responses in the first place. For strictly normal incidence, such modes are symmetry-forbidden. On the other hand, retardation makes the visualization of the resulting field lines slightly more complicated. It is responsible for the slight asymmetry noticeable between the front and back pairs of lobes in Fig. 2f. Most pronounced is the effect on the  $E_x$  field component, i.e., parallel to the excitation polarization. In our experiments, though, we are not sensitive to this component, as we discuss next.

Figure 3 shows typical nearfield optical microscopy images from a short-range ordered array of gold nanodisks. Two species of different diameters have been prepared on the same substrate to facilitate simultaneous imaging. The smaller disks were designed to be resonant at the excitation frequency with a dipolar response, while the larger ones are expected to exhibit a quadrupolar resonance. The shown images were obtained with different combinations of polarizations employed for excitation and analysis. In Fig. 3d clear signatures of dipolar and quadrupolar eigenmodes are discernable in direct correlation with disk diameters. Figure 3b does not offer such a simple and attractive interpretation. We have noticed in our studies with p-polarized excitation considerable variations in the resulting images, which we interpret as strong susceptibility to changing tip-sample interaction conditions.

This finding nicely corroborates our approach of using the cross-polarized near-field optical imaging scheme. In comparison with the numerical results from Fig. 2, we real-

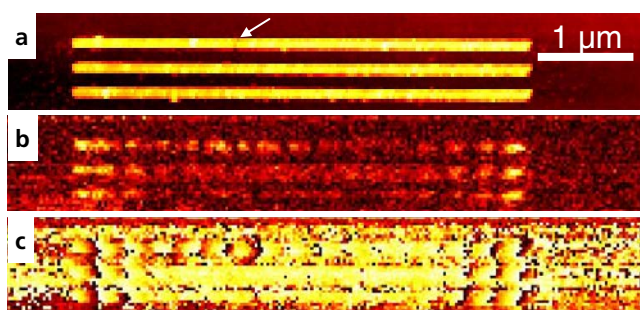


**Figure 4** Topography (a), near-field optical amplitude (b), and phase (c) images of simultaneously recorded plasmonic response of long gold wires excited with 875 nm radiation. The arrow in (a) indicates a structural defect.

ize that the recorded signal resembles the field component parallel to the probing tip shaft, i.e., normal to the sample surface. Taken together, these two observations – a clear correlation with structural parameters and the identification of the signal with the vertical field component – indicate a reliable, all-optical technique for the local study of plasmonic eigenmodes with superb spatial resolution and under ambient conditions.

In Fig. 3d, for instance, we may attribute deviations from the dipolar or quadrupolar behaviour expected from simulations to the presence of individual structural deformations. A slightly elliptic disk, whose main axes are not aligned with the parallel wavevector component, may explain nodal lines that are slightly rotated in the sample plane, and contaminating particular adsorbates may even distort the multipolar excitation pattern completely.

That the technique is not restricted to relatively small structures (on the scale of the exciting wavelength) is demonstrated in Fig. 4. Here, nominally identical gold wires of 5  $\mu\text{m}$  length are excited by 875 nm radiation. Infinitely long one-dimensional plasmonic structures exhibit damped, propagating wave phenomena [33, 34], whose dispersion largely depends on the geometry of the cross section, as well as on the nature of the embedding dielectric media. Intuitively, for wires of finite length standing wave like patterns are to be expected, which depend largely on the relative length scales given by the wire length, decay length, and undulation period.

In this vein, the eigenmodes observed at the lower two wires of Fig. 4 exhibit the damped interference pattern near the wire ends characteristic of a quasi semi-infinite wire, from which both the real and imaginary parts of the complex wavevector of one-dimensional waves along this wire structure can be determined. In the central parts of the wire, coupling of the incident excitation to such modes apparently is not strong enough to result in observable field strength. We note, however, the different behaviour of the top wire. In its left half, an additional standing wave pattern is observed,

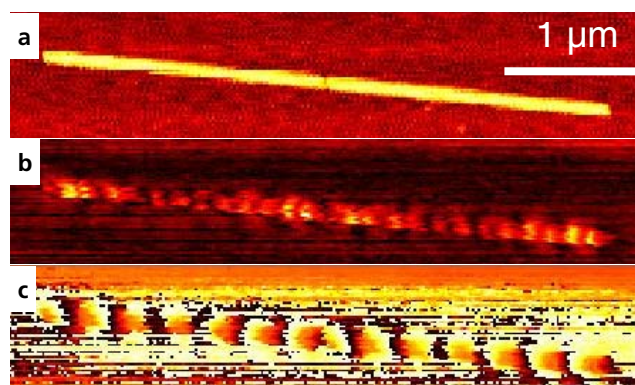


**Figure 5** Topography (a) and near-field optical amplitude (b) and phase (c) images of simultaneously recorded plasmonic excitations of a feed gap antenna structure consisting of two 2  $\mu\text{m}$  long wires with a gap of nominal 30 nm between them. Excitation wavelength:  $\lambda = 818$  nm.

which we associate with a structural defect hardly noticeable in the topography image.

In Fig. 5, such a “defect” was deliberately introduced as a 30 nm gap at the centre of a 4  $\mu\text{m}$  long wire. Acting like a feed gap antenna structure for radiation polarized along the length of the wires, it is expected to produce strong field enhancement in the gap. Clearly, the cross-polarized aSNOM reveals the excitation of a wave like pattern along the full length of the structure. It is expected to be anti-symmetric about the gap, but no particularly strong signature of any gap fields is observed. This comes as no surprise, when considered in the interpretation frame we have laid out above. The basic field component our technique is sensitive to is the one normal to the sample substrate surface. The enhanced fields in the gaps are oriented mostly horizontally, though. Thus, even if strong fields are present in the gap, a probe tip with its shaft oriented along the orthogonal direction will be essentially blind to these field components.

This finding is re-emphasized by Fig. 6, where the eigenmode of a relatively large bow tie antenna structure is shown. As before for wire antennas, from symmetry considerations it follows that the excitable plasmon mode should be anti-symmetric about the plane through the gap. This is nicely verified by the optical phase image. Consequently, in the central gap region we find only a weak local vertical field component.

Finally, we show that our cross-polarized aSNOM approach is also applicable to “inverse” plasmonic structures comprised of different kinds of holes or slots cut into a thin metallic film. Such structures fundamentally differ from the “positive” or “direct” structure we have discussed before. In addition to localised plasmonic modes, the extended film exhibits the well-known two-dimensional interface plasmon response, which is delocalized on the sample surface. This propagating plasmon mode leads to strong interference from or even coupling among the hole structure elements and thus much more pronounced collective excitations are possible.

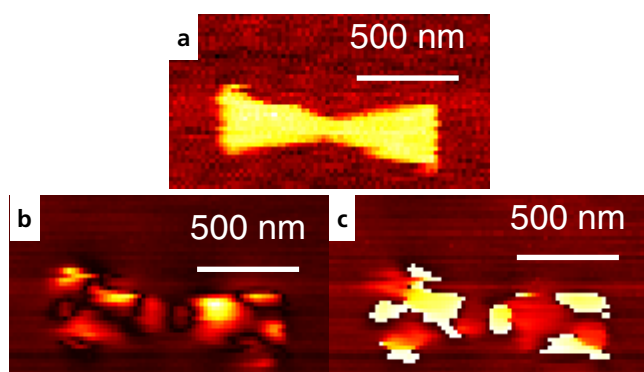


**Figure 6** Topography (a) and near-field optical amplitude (b) and phase (c) images of a bow tie antenna structure. Excitation wavelength:  $\lambda = 818$  nm.

A typical example is shown in Fig. 7. The arrangement of slots of variable length cut into a 250 nm thick gold film shows clear signatures of strongly localized excitations near the slots, especially in optical amplitude image. In regions away from the slot array the near-field optical patterns resemble those of damped propagating waves, as witnessed in the phase image by the trend of monotonic increase with distance (areas 2,3,4). Between arrays standing wave patterns are formed (area 1). A structural defect such as the one indicated by an arrow in (a) leads to the emission of approximately circular disturbance waves (area 3). An indication of the presence of more complicated collaborative effects is taken from the considerable number of phase singularities observed at several  $\mu\text{m}$  distance from the scattering structures (e.g. area 2). Evidently, the extended surface plasmonic modes do communicate interactions over distances of many times the inter-slot separations in this sample. The observed near-field optical patterns are likely not attributable to isolated single-slot mode excitations, but have to be understood as expressions of whole array modes.

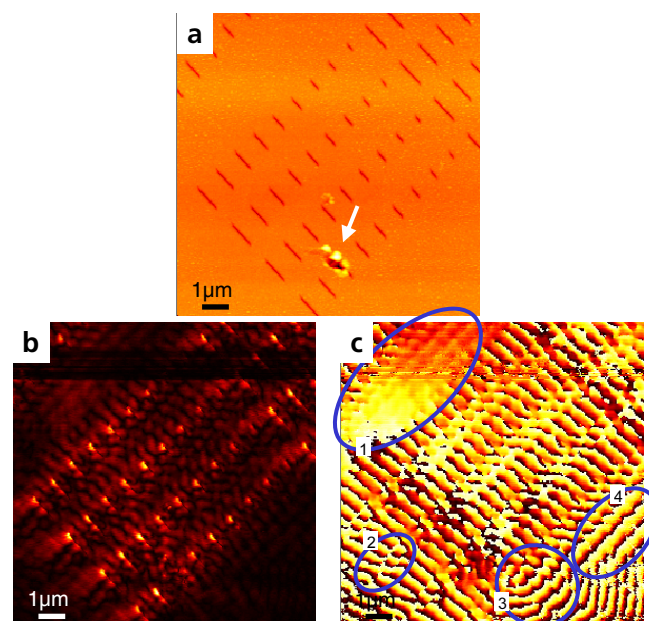


**Figure 7** Topography (a) and near-field optical amplitude (b) and phase (c) images of simultaneously recorded plasmonic excitations of a gold thin film, structured by FIB with an array of variable length slots. The excitation wavelength is  $\lambda = 773$  nm. The darker horizontal stripe in the upper half of (b) is due to a temporary drop in excitation power.

**4 Conclusions** In this paper we have shown that our combination of apertureless near-field optical microscopy with a cross-polarization scheme, which detects far-field radiation that is orthogonal to the excitation, yields a reliable technique to study local optical properties of resonant particle modes. A good interpretation of our images is pos-

sible by relating the recorded signal to the local vertical component of the complex electric field. Based on this rationale, recorded near-field optical images are readily interpreted with physical intuition. We are in the process of deriving from Maxwell's equations the necessary conditions for this rule to hold. In particular, the open question of how well a simple linear proportionality describes the relation between local fields (or their gradients) and recorded signal remains to be answered.

On the experimental side, the cross-polarization aSNOM has proven a versatile tool in many respects: it can be applied under ambient conditions to opaque as well as transparent sample types, direct and inverse, isolated confined structures as well as extended arrays. In particular, it facilitates the study of resonant plasmonic structures, whose eigenmode images are often severely distorted by local probes. This near-field optical approach will provide valuable information in fundamental research in the area of plasmonics and related optics. Also in an industrial context its capability to identify local structural distortions and the possibility to do combinatorial screening of many different manufacturing and/or design parameters with very few measurements will be of great benefit.

**Acknowledgements** The sample presented in Figure 7 has been provided by Hongcang Guo. The authors thank Prof. H. Giessen for stimulating discussions.

## References

- [1] S. Lal, S. Link and N. J. Halas, *Nature Photonics* **1**, 641 (2007).
- [2] P. Mühlischlegel, H.-J. Eisler, O. J. F. Martin, B. Hecht, and D. W. Pohl, *Science* **308**, 1607 (2005).
- [3] J. Aizpurua, P. Hanarp, D. S. Sutherland, M. Kall, G. W. Bryant, and F. J. G. de Abajo, *Phys. Rev. Lett.* **90**, 057401 (2003).
- [4] F. Hao, C. L. Nehl, J. H. Hafner, and P. Nordlander, *Nano Lett.* **7**, 729 (2007).
- [5] R. Bachelot, F. H'Dhili, D. Barchiesi, G. Lerondel, R. Fikri, P. Royer, N. Landraud, J. Peretti, F. Chaput, G. Larpel, J. P. Boilot, and K. Lahlil, *J. Appl. Phys.* **94**, 060 (2003).
- [6] A. Bouhelier, M. Beversluis, A. Hartschuh, and L. Novotny, *Phys. Rev. Lett.* **90**, 013903 (2003).
- [7] M. Thomas, J. J. Greffet, R. Carminati, and J. R. Arias-Gonzalez, *Appl. Phys. Lett.* **85**, 3863 (2004).
- [8] D. R. Smith, W. J. Padilla, D. C. Vier, S. C. Nemat-Nasser, and S. Schultz, *Phys. Rev. Lett.* **84**, 4184 (2000).
- [9] C. Rockstuhl, T. Zentgraf, H. Guo, N. Liu, C. Etrich, I. Loa, K. Syassen, J. Kuhl, F. Lederer, and H. Giessen, *Appl. Phys. B* **84**, 219 (2006).
- [10] T. Zentgraf, J. Dorfmueller, C. Rockstuhl, C. Etrich, R. Vogelgesang, K. Kern, T. Pertsch, F. Lederer, and H. Giessen, *Opt. Lett.* **33**, 848 (2008).
- [11] V. M. Shalaev, *Nature Photonics* **1**, 41 (2007).
- [12] A. Dmitriev, T. Pakizeh, M. Käll, and D. S. Sutherland, *Small* **3**, 294 (2007).
- [13] J. Nelayah, M. Kociak, O. Stephan, F. J. G. de Abajo, M. Tence, L. Henrard, D. Taverna, I. Pastoriza-Santos, L. M. Liz-Marzan, and C. Colliex, *Nature Phys.* **3**, 348 (2007).
- [14] E. J. R. Vesseur, R. de Waele, M. Kuttge, and A. Polman, *Nano Lett.* **7**, 2843 (2007).
- [15] F. Zenhausern, Y. Martin, and H. K. Wickramasinghe, *Science* **269**, 1083 (1995).
- [16] R. C. Dunn, *Chem. Rev.* **99**, 2891 (1999).
- [17] B. Knoll and F. Keilmann, *Nature* **399**, 134 (1999).
- [18] R. Hillenbrand and F. Keilmann, *Appl. Phys. B* **73**, 239 (2001).
- [19] N. Anderson, A. Bouhelier, and L. Novotny, *J. Opt. A Pure Appl. Opt.* **8**, 227 (2006).
- [20] K. G. Lee, H. W. Kihm, J. E. Kihm, W. J. Choi, H. Kim, C. Ropers, D. J. Park, Y. C. Yoon, S. B. Choi, H. Woo, J. Kim, B. Lee, Q. H. Park, C. Lienau, and D. S. Kim, *Nature Photonics* **1**, 53 (2007).
- [21] R. Hillenbrand, F. Keilmann, P. Hanarp, D. S. Sutherland, and J. Aizpurua, *Appl. Phys. Lett.* **83**, 368 (2003).
- [22] O. J. F. Martin and C. Girard, *Appl. Phys. Lett.* **70**, 705 (1997).
- [23] L. Novotny, R. X. Bian, and X. S. Xie, *Phys. Rev. Lett.* **79**, 645 (1997).
- [24] M. Micic, N. Klymyshyn, Y. D. Suh, and H. P. Lu, *J. Phys. Chem. B* **107**, 1574 (2003).
- [25] R. Hillenbrand and F. Keilmann, *Phys. Rev. Lett.* **85**, 3029 (2000).
- [26] L. Gomez, R. Bachelot, A. Bouhelier, G. P. Wiederrecht, S.-H. Chang, S. K. Gray, F. Hua, S. Jeon, J. A. Rogers, M. E. Castro, S. Blaize, I. Stefanon, G. Lereondel, and P. Royer, *J. Opt. Soc. Am. B* **23**, 823 (2006).
- [27] N. Ocelic, A. Huber, and R. Hillenbrand, *Appl. Phys. Lett.* **89**, 101124 (2006).
- [28] H. Fredriksson, Y. Alaverdyan, A. Dmitriev, C. Langhammer, D. S. Sutherland, M. Zäch, and B. Kasemo, *Adv. Mater.* **19**, 4297 (2007).
- [29] P. Hanarp, M. Kall, and D. S. Sutherland, *J. Phys. Chem. B* **107**, 5768 (2003).
- [30] A. Bek, R. Vogelgesang, and K. Kern, *Rev. Sci. Instrum.* **77**, 043703 (2006).
- [31] C. Hafner, *Max-1: A Visual Electromagnetics Platform* (Wiley, Chichester, 1998).
- [32] C. Hafner, *Post-Modern Electromagnetics: Using Intelligent Maxwell Solvers* (Wiley, Chichester, 1999).
- [33] G. W. Bryant, F. J. Garcia de Abajo, and J. Aizpurua, *Nano Lett.* **8**, 631 (2008).
- [34] L. Novotny, *Phys. Rev. Lett.* **98**, 266802 (2007).